

MICROCOPY RESOLUTION TEST CHART  
NATIONAL BUREAU OF STANDARDS 1963-A



AD-A156 608

# DEPARTMENT OF DEFENCE

DEFENCE SCIENCE AND TECHNOLOGY ORGANISATION

ELECTRONICS RESEARCH LABORATORY

DEFENCE RESEARCH CENTRE SALISBURY  
SOUTH AUSTRALIA

## TECHNICAL REPORT

ERL-0323-TR

A COMPACT BULK ACOUSTO-OPTIC TIME INTEGRATING CORRELATOR

D.A.B. FOGG

THE UNITED STATES NATIONAL  
TECHNICAL INFORMATION SERVICE  
IS AUTHORISED TO  
REPRODUCE AND SELL THIS REPORT

JUL 13 1984

DTIC FILE COPY

Approved for Public Release

Commonwealth of Australia  
NOVEMBER 1984

COPY No.

UNCLASSIFIED

AR-004-121

DEPARTMENT OF DEFENCE  
DEFENCE SCIENCE AND TECHNOLOGY ORGANISATION  
ELECTRONICS RESEARCH LABORATORY

TECHNICAL REPORT

ERL-0323-TR

A COMPACT BULK ACOUSTO-OPTIC TIME INTEGRATING CORRELATOR

D.A.B. Fogg

S U M M A R Y

This report describes the design and testing of a prototype correlator using lead molybdate Bragg cells. It indicates the suitability of this design for cells made of materials with longer transition times, such as tellurium dioxide. Compactness and simplicity are achieved by the use of a specially designed prism: An analysis of the AO, TIC process and performance parameters is given.



---

POSTAL ADDRESS: Director, Electronics Research Laboratory,  
Box 2151, GPO, Adelaide, South Australia, 5001.

---

UNCLASSIFIED

## TABLE OF CONTENTS

	Page
1. INTRODUCTION	1
2. TIC ARCHITECTURE	1
3. TIC ANALYSIS	2
4. THE PRISM	7
4.1 Design geometry	7
4.2 The effect of rotation	8
4.3 Crossover distance	9
4.4 Coating	9
5. EXPERIMENTAL RESULTS	10
6. PERFORMANCE	13
7. CONCLUSIONS	14
8. ACKNOWLEDGEMENT	15
NOTATION	16
REFERENCES	18

## LIST OF APPENDICES

I DETERMINATION OF PRISM CHARACTERISTICS	20
II REVIEW OF PERFORMANCE PARAMETERS	24

## LIST OF TABLES

1. PRISM DIELECTRIC COATINGS	10
2. TEST RESULTS	13
3. PERFORMANCE PARAMETERS	14

## LIST OF FIGURES

1. Bragg cell orientation	<i>11</i>
2. Bulk AO TIC correlator architecture	<i>11</i>
3. Bragg cell optics	<i>11</i>
4. The prism	<i>11</i>



ERL-0323-TR

5. Incidence angle sensitivity
6. Signal and noise spectra
7. Dynamic range limits, two tone case
8. Correlator output for an OOK signal
- 9(a). Correlator output for a spread spectrum signal
- 9(b). Phase shifted output for pedestal subtraction
10. Correlation peak after digital subtraction
11. Prism geometry
12. Prism rotation geometry
13. Crossover distance

## 1. INTRODUCTION

Acousto-optical (AO) signal correlators have been described and discussed extensively in past literature (ref.1 to 5). Compactness is often of prime importance in such devices. This report describes a dual beam bulk acousto-optic time integrating correlator (TIC) in which compactness and simplicity are achieved by use of a specially designed prism. The shape and transmission coating permit the direction of laser beams of the correct intensity, angular separation and polarisation through two Bragg cells. Unknown and reference signals supplied to these cells modulate the incoming light. A CCD linear photodiode array detector is used to sum and square the modulated light. The detector output contains the desired correlation.

Correlator analysis is usually simplified by using analytic signal equivalents and omitting the optical beam expression. A fuller analysis is given in Section 2. Although more laborious, it leads to a better understanding of the process.

Specifications for the prism vary with Bragg cell type. Prism parameters are described analytically, enabling practical construction details to be calculated to suit any Bragg cell.

The correlator architecture is described. A prototype was made using available lead molybdate cells and experimental results are given for the correlation of a number of signals. Performance criteria are discussed in Section 6, and the bases for these criteria are reviewed in Appendix II.

## 2. TIC ARCHITECTURE

In bulk AO TIC correlators, the deflected first order beam of one cell may be spread and introduced at the Bragg angle to the second cell. The deflected beam from the second cell contains the information which on integration at the detector, provides the desired correlation. Alternatively, separate first order beams from each cell can be produced and combined by reflection or refraction. Surface acoustic wave devices have been designed (ref.7) to produce two collinear first order beams. The architecture developed here produces collinear first order beams from bulk AO devices using a specially designed prism, resulting in an efficient compact assembly.

If the direction of the incident laser beam to a Bragg cell has a component in the direction of propagation of the acoustic strain wave in the cell, the deflected light is downshifted in frequency and is referred to as the -1th order (ref.3). Alternatively, if the incident beam has a component in the opposite direction to the acoustic strain wave a +1th order (upshifted) deflected beam is obtained. By orientating two Bragg cells, and choosing appropriate acoustic propagation directions it is possible to obtain identically shifted collinear deflected beams, one from each cell. Figure 1 shows the required arrangement to achieve either upshifted or downshifted collinear first orders. In both cases, the angle between the cell axes is twice the Bragg angle and the two incident beams have a divergence of four times the Bragg angle.

The deflected  $+1_A$  and the undeflected  $0_A$  beams from the first cell pass through the second cell, B. The  $0_A$  beam makes an angle  $3\theta_B$  with cell B. This is not close enough to the Bragg angle to give rise to further deflected beams and it is transmitted virtually unchanged. The  $+1_A$  beam incident on cell B at  $\theta_B$  gives rise to a deflected beam coincident with  $0_B$ . It suffers a small intensity loss equal to the deflection efficiency. (Of the order of 8% for

the lead molybdate cells and the RF power used.)

The correlator is shown schematically in figure 2. A beam from a 10 mW laser was spatially filtered and expanded to provide a 10 mm wide by 1 mm high beam. P-polarisation was used (ie the electric vector in the plane of incidence) to optimise the performance of the Bragg cells. A phase equalising plate was used in one half of the beam. This plate could be rotated  $5^\circ$  to obtain a full  $360^\circ$  phase change. The prism produced two equal intensity 10 mm x 1 mm beams diverging at an angle of  $4\theta_B$  but precisely in the same horizontal plane. The undeflected beams were stopped shortly after separating from the coincident first orders. A 1024 element CCD array was used as the detector.

### 3. TIC ANALYSIS

The RF signal modulated in amplitude and phase and directed to the Bragg cell transducer can be denoted by,

$$s(t) = A(t) \cos\{2\pi f_c t + \alpha(t)\} \quad (1)$$

$$= \text{Re} \{A(t) \exp j [2\pi f_c t + \alpha(t)]\} \quad (2)$$

where Re denotes "the real part of".

Within the cell this driving waveform is given by(ref.3)  $s(t - x/v)$  or  $s(t + x/v - T)$  where  $v$  is the acoustic velocity within the cell and  $T$  is the transit time (cell width divided by acoustic velocity). The former expression represents sound wave propagation in the positive direction and the latter the reversed propagation.

The object is to find the autocorrelation function  $R_{ss}(\tau)$  of the signal  $s(t)$ . It is possible to simplify the analysis by considering the signal's associated analytic function given by

$$\left. \begin{aligned} z(t) &= s(t) + j \hat{s}(t) \\ \text{or} \\ z(t) &= A(t) \exp j[2\pi f_c t + \alpha(t)] \end{aligned} \right\} \quad (3)$$

for  $s(t)$  given by equation (2)

Here  $\hat{s}(t)$  is the Hilbert transform of  $s(t)$ (ref.8). The envelope  $\epsilon(t)$  of  $z(t)$  is obtained by multiplying by  $\exp(-j2\pi f_c t)$  (ie extracting the carrier) so that

$$\epsilon(t) = z(t) \exp(-j2\pi f_c t) \quad (4)$$

The Fourier transforms  $S(\omega)$ ,  $Z(\omega)$  and  $E(\omega)$  of  $s(t)$ ,  $z(t)$  and  $\epsilon(t)$  respectively are related by(ref.8)

$$Z(\omega) = \begin{cases} 2 S(\omega) & \omega > 0 \\ 0 & \omega < 0 \end{cases} \quad (5)$$

and

$$E(\omega) = Z(\omega + \omega_0), \quad \omega_0 \approx 2\pi f_c$$

Therefore if the spectrum  $E(\omega)$  of the envelope is confined to the positive region,  $\varepsilon(t)$  contains the information concerning the slow amplitude and phase variations of the signal  $s(t)$  and satisfies the intuitive concept of an envelope (ie the carrier frequency  $f_c$  is greater than the highest frequencies occurring in the information component of the signal).

It is not sufficient to find the autocorrelation function  $R_{\varepsilon\varepsilon}(\tau)$  of this envelope since it is not equal to the autocorrelation function  $R_{SS}(\tau)$  of the real signal. They are related by

$$R_{\varepsilon\varepsilon}(\tau) = R_{ZZ}(\tau) \exp(-j 2\pi f_c \tau) = 2[R_{SS}(\tau) + j \hat{R}_{SS}(\tau)] \quad (6)$$

where  $\hat{R}_{SS}(\tau)$  is the Hilbert transform of  $R_{SS}(\tau)$  (ref. 8). Therefore

$$R_{SS}(\tau) = \frac{1}{2} \text{Re} \{R_{\varepsilon\varepsilon}(\tau)\} \quad (7)$$

A number of authors (ref.3) for example treat the case where the analytic signal  $z(t)$  or a complex equivalent to  $s(t)$  is assumed to be the input to the TIC. The output is usually shown as,

$$O(t) = \int_{t_0}^{t_1} \left| \frac{1}{2} jz(t - x/v) + \frac{1}{2} jz(t + x/v - T) \right|^2 dt \quad (8)$$

Expanding, this becomes

$$\begin{aligned} O(t) = & \frac{1}{4} \int_{t_0}^{t_1} z^2(t - x/v) dt + \frac{1}{4} \int_{t_0}^{t_1} z^2(t + x/v - T) dt \\ & + \frac{1}{2} \int_{t_0}^{t_1} \text{Re} \{z(t - x/v) z^*(t + x/v - T)\} dt \end{aligned}$$

where  $t_1 - t_0$  is the integration time.

The last term is  $\frac{1}{2} \text{Re} \{R_{ZZ}(2x/v - T)\}$ . From equation (6)

$$(\exp j2\pi f_c \tau) R_{zz}(2x/v - T) = 2[R_{ss}(2x/v - T) + j \hat{R}_{ss}(2x/v - T)] \quad (9)$$

so that

$$\frac{1}{2} \operatorname{Re} \{R_{zz}(2x/v - T)\} = R_{ss}(2x/v - T) \quad (10)$$

It is then implied that using the real signal instead of the analytic one will produce the same term.

It is instructive to consider this process in more detail, incorporating the direction of propagation of the light and delaying use of analytical functions until after an expression for the output light is obtained. The laser beam incident on one face of a Bragg cell can be represented by the coherent plane wave

$$L(\underline{r}, \underline{d}, t) = \operatorname{Re} \{a \exp j 2\pi(vt - 1/\lambda \underline{r} \cdot \underline{d})\} \quad (11)$$

where  $\underline{r} = x\underline{i} + z\underline{k}$  is the position vector of a point P in space (see figure 3)

$\underline{d} = \sin \theta \underline{i} + \cos \theta \underline{k}$  is a unit vector in a fixed direction.

and  $\lambda$  is the wavelength of light in the medium of propagation. The quantity  $L(\underline{r}, \underline{d}, t)$  represents a plane wave since it is constant over the plane  $\underline{r} \cdot \underline{d}$  at any time  $t$ .

The optical output of the Bragg cell is determined by assigning to it a transmittance  $tr(x, t)$  equivalent to that of a sinusoidal phase grating (see reference 9)

$$tr(x, t) = (C_0 \exp js(t - x/v)) \quad (12)$$

where  $C_0$  is a function of the incidence angle  $\theta_i$  and represents the strength of interaction. The deflected output  $U(x, t)$  is therefore using equation (2),

$$U(x, t) = \operatorname{Re} \{a \exp j 2\pi(vt - 1/\lambda \underline{r} \cdot \underline{d}')\} C_0 \exp js(t - x/v)$$

where  $\underline{d}'$  is  $\underline{d}$  with the sign of the  $i$ th component chosen to account for the deflection of the light beam. Expanding the second exponential and taking the first two terms this becomes

$$U(x, t) = \operatorname{Re} \{a \exp j 2\pi(vt - 1/\lambda \underline{r} \cdot \underline{d}')\} C_0 [1 + js(t - x/v)]$$

The deflected light  $U'(x, t)$  is represented by the second term in the square brackets. This can be written

$$U'(x, t) = \operatorname{Re} \{a \exp j 2\pi(vt - 1/\lambda \underline{r} \cdot \underline{d}')\}$$

$$j C_0 \operatorname{Re} \{A(t - x/v) \exp j[2\pi f_c(t - x/v) + \alpha(t - x/v)]\}$$

Substituting for  $\underline{r}$  and  $\underline{d}$  and using the relationship

$$\text{Re} \{ \exp j\theta_1 \} \text{Re} \{ \exp j\theta_2 \} = \frac{1}{2} \text{Re} \{ \exp j(\theta_1 + \theta_2) + \exp j(\theta_1 - \theta_2) \}$$

this becomes,

$$\begin{aligned} U'(x,t) = & \frac{1}{2} aA(t - x/v) \text{Re} \left\{ C_o \exp j \left[ 2\pi(\nu + f_c)t + \alpha(t - x/v) \right. \right. \\ & \left. \left. - 2\pi \left( \frac{nx}{\lambda_o} \sin \theta_i + \frac{nz}{\lambda_o} \cos \theta_i - f_c x/v \right) \right] \right\} \\ & + C_o \exp j \left[ 2\pi(\nu - f_c)t - \alpha(t - x/v) \right. \\ & \left. + 2\pi \left( \frac{nx}{\lambda_o} \sin \theta_i - \frac{nz}{\lambda_o} \cos \theta_i + f_c x/v \right) \right] \left. \right\} \end{aligned}$$

Here  $\lambda_o = n\lambda$ ,  $\lambda_o$  is the light wavelength in vacuo and  $n$  is the refractive index of the Bragg cell material. This represents two sidebands, one at an upshifted optical frequency  $(\nu+f)$  and the other downshifted to  $(\nu-f)$ . When the angle of incidence  $\theta_i$  is  $\pm\theta_B$ , the Bragg angle, one of these sidebands is maximised and the other disappears ( $C_o = 0$  or  $C'_o = 0$ ).

Consider the upshifted sideband  $U_1(x,t)$  is equation (5). This has the form

$$U_1(x,t) = \frac{1}{2} j aA(t - x/v) \cos[2\pi(\nu + f_c)t + \alpha(t - x/v) + C_1(x)] \quad (13)$$

where

$$C_1(x) = -2\pi \left[ \frac{nx}{\lambda_o} \sin \theta_i + \frac{nz}{\lambda_o} \cos \theta_i - f_c x/v \right]$$

Notice that this is not identical to  $s(t - x/v)$ . The carrier is now  $\nu + f_c$  and there is an additional phase term  $C_1(x)$  related to the spatial progression of the signal across the cell.

From the other cell the output can be shown to be

$$U_2(x,t) = \frac{1}{2} j aA(t + x/v - T) \cos[2\pi(\nu + f_c)t + \alpha(t + x/v - T) + C_2(x)] \quad (14)$$

where

$$C_2(x) = 2\pi \left[ \frac{nx}{\lambda_o} \sin \theta_i - \frac{nz}{\lambda_o} \cos \theta_i + f_c x/v - f_c T \right]$$

The output  $U_1$  and  $U_2$  are added coherently and the intensity registered by the detector is the square of this sum. This is integrated for a time  $t_1 - t_o$ , producing an output voltage proportional to

$$\int_{t_0}^{t_1} |U_1(x,t) + U_2(x,t)|^2 dt \quad (15)$$

Since  $U_1$  and  $U_2$  contain phase terms it is difficult to eliminate the carrier. The best way of interpreting equation (15) is via analytic functions. The analytic function associated with  $U_1(x,t)$  is given by

$$z_1(t - x/v) = \frac{1}{2} a A(t - x/v) \exp j[2\pi(\nu + f_c) + \alpha(t - x/v) + C_1(x)] \quad (16)$$

A corresponding expression exists for  $U_2$ . Replacing  $U_1$  and  $U_2$  in equation (15) by  $z_1$  and  $z_2$

$$I = \int_{t_0}^{t_1} |z_1(t - x/v) + z_2(t + x/v - T)|^2 dt \quad (17)$$

but from equation (3)

$$z(t - x/v) = A(t - x/v) \exp j[2\pi f_c(t - x/v) + \alpha(t - x/v)]$$

so that from equation (16)

$$z_1(t - x/v) = \frac{1}{2} j a \exp j 2\pi \nu t \exp j C'_1(x) z(t - x/v)$$

where

$$C'_1(x) = C_1(x) + f_c x/v$$

and similarly

$$z_2(t + x/v - T) = \frac{1}{2} j a \exp j 2\pi \nu t \exp j C'_2(x) z(t + x/v - T)$$

where

$$C'_2(x) = C_2(x) - f_c x/v + f_c T$$

Therefore I becomes

$$I = \frac{1}{4} a^2 \int_{t_0}^{t_1} |\exp j 2\pi\nu t|^2 |z(t - x/v) \exp C'_1(x) + z(t + x/v - T) \exp j C'_2(x)|^2 dt$$

Since  $|\exp j\theta| = 1$  for real  $\theta$ , this can be expanded as

$$I = \frac{1}{4} a^2 \int_{t_0}^{t_1} |z(t - x/v)|^2 dt + \frac{1}{4} a^2 \int_{t_0}^{t_1} |z(t + x/v - T)|^2 dt + \frac{1}{2} a \operatorname{Re} \int_{t_0}^{t_1} z(t - x/v) z^*(t + x/v - T) dt \quad (18)$$

The last integral has already been considered following equation (9), and is the desired autocorrelation function  $R_{SS}(2x/v - T)$  multiplied by the light intensity constant,  $a$ . If the integration time is large compared with  $1/f_c$  the first two integrals of equation (18) are constant depending only on the integration time  $(t_1 - t_0)$ . The expression equation (18) is therefore of the form

$$I = \text{bias} + R_{SS}(2x/v - T) \quad (19)$$

This result is also produced by the integral in equation (15). Thus the TIC is seen to produce the desired autocorrelation function in a time frame compressed by a factor of 2. Both amplitude and phase modulation in the signal are seen to be preserved during processing by the Bragg cell. The initial RF carrier of frequency  $f_c$  is replaced by a light carrier of frequency  $\nu + f_c$  (or  $\nu - f_c$ ). The correlation function is then formed by coherent summation, squaring and integration in the detector. The analysis shows that the correlator can be used with pure amplitude modulated, ( $\alpha(t) \equiv 0$ ), pure phase modulated signals ( $A(t) \equiv 1$ ) or both amplitude and phase modulated signals. This is discussed further in Section 5.

#### 4. THE PRISM

The prism is required to superimpose two parts of a polarised spread laser beam each 10 mm horizontally by 1 mm giving rise to two beams with a resultant divergence of  $4\theta_p$ , and equal intensities. One beam (see figures 11 and 4) enters surface 3 at normal incidence, is reflected from surface 2 and emerges from surface 1. The second beam undergoes a reflection from surface 1.

##### 4.1 Design geometry

The prism is defined by any four of the angles given below, where the angle between surface  $i$  and  $j$  is denoted by  $\alpha_{ij}$  (see Appendix I)

$$\begin{aligned}
\alpha_{12} &= \frac{1}{2}(\pi/4 + \theta_B) - \frac{1}{2} \sin^{-1} [\sin(\pi/4 - 3\theta_B)/n] \\
\alpha_{13} &= 3\pi/4 - \theta_B \\
\alpha_{14} &= \sin^{-1} [\sin(\pi/4 - 3\theta_B)/n] \\
\alpha_{32} &= \frac{1}{2} \sin^{-1} [1/n \sin(\pi/4 - 3\theta_B)] + \pi/8 + \frac{1}{2}\theta_B \\
\alpha_{35} &= \pi/2
\end{aligned} \tag{20}$$

Here  $n$  is the refractive index of the glass used in the prism.

A prism was manufactured in the DRCS optical laboratories for use with lead molybdate Bragg cells. Type BK7 glass was used and the surfaces were ground and polished to reduce wavefront distortion at each surface to better than  $\lambda/10$  for  $\lambda = 632.8$  nm. Since the Bragg cell output is sensitive to the incident angle (see figure 5) an attempt was made to make the prism angles as precisely as possible. The actual angles achieved were measured using a goniometer and were found to be within 2" of the desired values. Pyramidal error was of prime concern. No pyramidal error could be observed in the final product. Details of the phase corrector plate used to compensate for the effects of path differences between the two beams are given in Appendix I.

#### 4.2 The effect of rotation

In order to accommodate variation in Bragg angle and slight errors in achieving the required prism angles, the prism can be rotated. This changes the divergence of the two outgoing beams. The relation between prism rotation  $\Delta\theta$  and beam divergence  $\phi$  is derived in Appendix I.

For small  $\Delta\theta$  this reduces approximately to a simple linear relationship

$$\phi = C_0 \Delta\theta + C_1 \tag{21}$$

For lead molybdate  $C_0 = 0.78 (\pm 0.02)r$  and  $C_1 = 0.028r (=4\theta_B)$ . The prism can also be placed on a goniometer and rotated relative to the incident beam until the output beam divergence is precisely  $4\theta_B$ .

A mathematical model of the Bragg cell (ref.11) based on the Klein and Cook analysis (ref.10) was used to produce a graph of the relationship between output intensity and angle of incidence for the lead molybdate cell using a wavelength of  $\lambda = 632.8$  nm. This is shown in figure 5 together with experimental values.

This function is the Fourier transform of the rectangular aperture of the incident beam. At the peak a rotation of  $\delta\alpha = 1.4$  mrad (5 ft) produces a detectable decrease in intensity. To avoid reducing the sensitivity of the system the prism manufacturing tolerances need to ensure that the divergence is within  $\pm\delta\alpha$  of  $2\theta_B$ . The actual error was 0.02 mrad (4") and in the next section it is shown that this error can be made arbitrarily small by rotation of the prism. The prism therefore does not limit the performance of the system.

### 4.3 Crossover distance

To achieve the desired collinearity of the deflected beams the crossover point of the two input beams should be between the two Bragg cells. The crossover point can be adjusted by varying the relative position of the beams entering the prism. This point can readily be determined by trial and error once the prism has been manufactured. However, it is preferable to ensure that the appropriate crossover distance is achievable when specifying the prism dimensions before manufacture. The crossover distance  $d_c$  of two rays, one in each beam is given by, (see figure 13)

$$d_c = \sin(\xi - 2\theta_B) \{ (x_D - x_G)^2 + (Y_D - Y_G)^2 \}^{1/2} / (2 \sin 2\theta_B)$$

where

$$\xi = \pi - \alpha_{31}, \quad \gamma = \alpha_{32}$$

$$x_D = \{ (S_3 - S_1) \tan \gamma + (S_3 - S_1) \cot 2\gamma + S_3 \tan \xi \} / (\cot 2\gamma + \tan \xi)$$

$$Y_D = (x_D - S_3) \tan \xi$$

$$x_G = S_3 + S_2$$

and

$$Y_G = S_2 \tan \xi .$$

For a given prism this can be reduced to a simple relationship namely,

$$d_c = C_1 S_2 + C_2$$

where  $C_1$  and  $C_2$  are constants.

### 4.4 Coating

Surfaces 1, 2 and 3 were coated to satisfy relative beam intensity requirements. Surface 4 was coated for maximum transmission out of the prism. Surfaces 5, top and bottom were not polished.

Denoting the transmittance and reflectance of the  $i$ th prism surface by  $t_i$  and  $r_i$  respectively, the design requirement of equal beam intensity is  $t_3 r_2 t_1 = r_1$ , given  $n$ ,  $\lambda$ , and p-polarisation. Surface 3 was antireflection coated, ( $t_3 = 1$ ). Because the angle of incidence at surface 2 was almost the Brewster angle, a dielectric stack was impractical. An aluminium coating was used and therefore  $r_2 = 0.83$ (ref.12). For a dielectric stack  $r + t = 1$ . It follows that  $t_1 = 0.55$  and  $r_1 = 0.45$ . Coating details are

given in Table 1. The measured beam intensities of the coated prism were within 1%.

TABLE 1. PRISM DIELECTRIC COATINGS

Surface	Layer	Material	Optical thickness, (nm)
3	1	ZrO <sub>2</sub>	380
	2	MgF <sub>2</sub>	140
1	1,3,5	MgF <sub>2</sub>	180
	2,4,6	ZrO <sub>2</sub>	180

### 5. EXPERIMENTAL RESULTS

TIC correlators can process a variety of signals including CW, linear FM and direct sequence types(ref.7). It is instructive to use both amplitude modulated and phase modulated signals to test the system. As examples of pure amplitude modulated signals, on-off-keyed pulsed CW (OOK/CW) signals were used. These produce regular correlation pulses across the detector indicating the degree of apodisation. As examples of pure phase modulated signals, on-off-keyed binary phase shifted (OOK/BPSK) and spread spectrum binary phase shift keyed (SPREAD/BPSK) signals were used. The former for comparison with the OOK/CW signals and the latter as examples of single correlation peak output.

For these cases the input signals  $s(t)$  given in general by equation (1) become(ref.13)

$$\text{OOK/CW} \quad s_1(t) = \sum_{n=-\infty}^{\infty} \text{rect} \left[ \frac{t - nT}{t_p} \right] \cos 2\pi f_c t \quad (22)$$

$$\text{OOK/BPSK} \quad s_2(t) = \sum_{n=-N/2}^{N/2} \{ 2 s_o(t - 2nt_p) - s_o(t - nt_p) \} \quad (23)$$

$$\text{SPREAD/BPSK} \quad s_3(t) = \sum_{n=-N/2}^{N/2} (2a_n - 1) s_o(t - nt_p) \quad (24)$$

where  $s_o(t) = \text{rect } t \sin 2\pi f_c t$ ,  $f_c \ll 1/t_p$ ,  $-t_p/2 < t < t_p/2$ , and  $t_p$  is the pulse duration. The terms  $a_n$  are either zero or one and form a linear recursive sequence (LRS).  $s_1(t)$  was synthesised using a signal generator and a device was built to phase shift a suitable carrier to obtain  $s_2(t)$ . For the spread spectrum, pseudo noise signal  $s_3(t)$ , a 127 bit (R7) LRS code was generated using a shift register with appropriate feedback. The LRS generator was defined by the polynomial  $x^7 + x^1 + x^0 = 0$ . By adding the output (modulo 2) from the last two register positions an identical LRS with lag 7 was obtained and used to generate the reference pseudonoise signal.

The circuit design allowed for modulation rates of  $f_c/2^s$ ,  $s = 1, 2, \dots, 7$ . The observable lag between the reference and test signals was restricted to the cell transit time divided by the pulse duration  $\tau/t_p$  (see Table 3).

The normalised autocorrelation functions for the above signals are(ref.13):

$$\text{OOK/CW and BPSK } R_{s_1s_1}(\tau) = R_{s_2s_2}(\tau) = \sum_{n=-N/2}^{N/2} \text{rect} \frac{t-2nt_p}{t_p} \left(1 - \frac{|\tau|}{t_p}\right) \quad (25)$$

$$\text{SPREAD/BPSK } R_{s_3s_3}(\tau) = \begin{cases} 1 - \frac{2^N}{2^{N-1}} \frac{|\tau|}{t_p} & |\tau| \leq t_p \\ \frac{1}{2^{N-1}} & |\tau| > t_p \end{cases} \quad (26)$$

The correlation peaks are triangular in shape. The OOK signals produced peaks at every second bit position across the cell, (see figure 8). The spread signals each produced a simple correlation peak one bit wide, readily discernable above the pedestal, (see figure 9). The pedestal showed indications of aperture diffraction, the Gaussian laser profile and a periodic interference due to a transparent cover over the detector elements. The latter could be removed by using a detector without a sealing window. Pedestal subtraction can be used to largely remove the effect of the pedestal. Figure 9(a) shows the normal correlator output peak. Figure 9(b) shows the output when a 180° phase delay was incorporated into the reference RF signal. Subtracting the two removes the pedestal and increases the height of the correlation peak. Subtraction was implemented by digitising the output of the 1024 element linear photodiode array using a 12 bit analog-to-digital converter. The conversion time was 2.8  $\mu$ s giving a 3 ms scan rate. The results were stored on HP85 computer disc files. The results of the pedestal subtraction are shown in figure 10. With better beam shaping optics and a windowless detector the base would be as flat as the outer edges of figure 10(c).

The test cases run and the results observed are shown in Table 2.

TABLE 2. TEST RESULTS

Switch (s)	Division factor (2 <sup>S</sup> )	Modulation rate $\Omega = f_c / 2^S$ (MHz)	Pulse duration $t_p = 1/2\Omega$ ( $\mu$ s)	Chip rate $T_c = 1/t_p$ (MHz)	Maximum lag (pulses in cell)	Correlation peak*		
						BPSK/ OOK (mV)	BPSK SPREAD (mV)	Pulsed CW (mV)
2	4	19.5	0.026	39.0	105	>200	>100	>400
3	8	9.8	0.05	19.5	52	>200	>400	>400
4	16	4.9	0.10	9.8	26	>200	>300	>300
5	32	2.4	0.21	4.9	12	>200	>300	>300
6	64	1.2	0.41	2.4	6	>200	NA	NA
7	128	0.61	0.82	1.2	3	-	NA	NA

$$f_c = 78 \text{ MHz, transit time of cell} = 2.7 \mu\text{s}$$

\* See figures 8, 9 and 10 to obtain an indication of S/N ratio

## 6. PERFORMANCE

The input signal to a correlator will be contaminated by noise so that the output, equation (15), will be of the form

$$\int_{t_2}^{t_1} |U_1(x,t) + n(t) + U_2(x,t)|^2 dt \quad (27)$$

In a correlator, the energy from a spread signal is concentrated into a narrow output pulse. The total energy of the noise is unchanged by the correlator, but spread in frequency since the spectrum of the noise X signal product is the convolution of the noise and signal spectra. The noise in the signal bandwidth is reduced. Figure 6(a) shows the changes in signal and noise spectra brought about by the correlator, for the case of a spread spectrum signal and broadband noise. Figure 6(b) shows the narrow band noise case.

Since AO correlators are essentially equivalent to matched filters, the well known assessments of matched filter performance are applicable (ref.14,15). The enhancement of signal to noise ratio (ie processing gain) achieved is given by the product of the effective duration of the signal correlated and its bandwidth. Review of classical and current estimates of processing gain are given in Appendix II.

The processing gain PG of a spatial integrating correlator is limited to the product,  $B\tau$ , of the Bragg cell bandwidth  $B$ , and its transit time  $\tau$ . In a time integrating correlator, the factor limiting PG is either the dynamic range  $R$  of the detector, or the inherent PG of the signal, whichever is the smallest. In the former case, it can be shown (ref.1) that the "effective" time bandwidth product for a TIC is  $R^2$ . In a TIC the transit time limits the observable lag between reference and test signals. The maximum observable lag is the cell transit time divided by the pulse duration,  $t_p$ . For a 10 MHz chip rate  $t_p = 0.1 \mu\text{s}$ . For the prototype correlator  $\tau = 3 \mu\text{s}$  allowing a maximum lag of 30 pulses. In many applications much larger maximum lags are required necessitating Bragg cells with larger apertures. Tellurium dioxide cells currently offer the largest apertures at low frequencies when operated in the

slow shear propagation mode. ERL has recently purchased two types of tellurium dioxide cells with apertures of 50  $\mu$ s and 70  $\mu$ s and it is proposed to construct correlators using these cells which will have maximum lags of 500 and 700 pulses respectively. Dynamic range, including the Bragg cell's inherent dynamic range, is discussed in more detail in Appendix II.

TABLE 3. PERFORMANCE PARAMETERS

Bragg cell type	Frequency range (MHz) fmin cf fmax	Bandwidth (MHz)	Transit time (s)	Time bandwidth product	Resolution $\frac{1}{\tau}$	Maximum lag at 10 MHz chip rate (pulses)
Lead Molybdate	60 80 100	40	3	120	333 kHz	30
Tellurium dioxide deflector	30 45 60	30	50	1500	20 kHz	500
Tellurium dioxide deflector	35 50 65	30	70	2100	14 kHz	700

Detector dynamic range 500:1

Frequency resolution  $\delta f$  is determined by the width D of the light beam.  $\delta f = v/D$  where v is the velocity of sound in the cell. Resolution is best when D is the width of the cell and then  $\delta f = 1/\tau$ . Typical values for the lead molybdate cell used in the prototype TIC, and the proposed tellurium dioxide correlator (50  $\mu$ s or 70  $\mu$ s) are shown in Table 3.

### 7. CONCLUSIONS

In this report, a specific bulk AO TIC design has been described. It features collinear deflected first order beams. This has a number of distinct advantages. It ensures coplanar optical wavefronts at the detector eliminating the Young's fringes seen in some designs. It also avoids the need for 2 additional lenses and a frequency plane stop after the Bragg cells to eliminate the undeflected beams. In this architecture, the deflected and undeflected beams are separated by their natural divergent propagation. No similar correlator architecture has been reported in the literature on bulk AO time integrating correlators.

The prism used in the correlator is also novel and facilitates the directing and intensity control of the correlator's input laser beams. Analytic expressions defining the prism have been given. These enable the manufacturing specifications of a prism for any Bragg cell to be readily defined, taking full account of its Bragg angle and polarisation requirements. The prism would also be useful in other bulk AO and Opto-SAW architectures. The effect of rotation of the prism has been well defined. It causes a variation in divergence of the output beams. Because of this, a prism made to a given specification can be used with a range of different Bragg cells. The variation in beam divergence can be calculated from the analytic expressions provided. The essential requirement that the crossover point of the input beams lies between the two Bragg cells has been incorporated into the design of the prism and the relevant equations defining crossover distance have been provided.

The analysis of the correlator includes expressions for the light beams and

provides a level of detail not reported explicitly in the literature. This gives a clear understanding of the processes involved, particularly in the case of phase modulated signals.

Experimental results obtained from a prototype built from available lead molybdate cells confirmed the usefulness of the design. Longer transit time cells can be used. This would increase the maximum lag between unknown and reference signals. The use of 50  $\mu$ s or 70  $\mu$ s tellurium dioxide cells in this architecture would result in a practical, compact time integrating correlator suitable for use with a variety of signals. It would have a large potential processing gain, currently limited by the state of the art CCD linear photodiode arrays but capable of readily taking advantage of advances in this area.

#### 8. ACKNOWLEDGEMENT

The author wishes to acknowledge with thanks the members of Optical Techniques group at ERL who manufactured the prism and Mr J. Venning of the same group who designed the prism coatings.

NOTATION

$a_n$	nth term in LRS
$A(t)$	amplitude
$B$	bandwidth
$\underline{d}$	unit vector
$d_c$	crossover distance
$E$	energy in signal $s(t)$
$E(\omega)$	Fourier transform of $\varepsilon(t)$
$f$	frequency
$f_c$	carrier frequency
$\underline{i}$	unit vector, x direction
$J_i$	Bessel function of order $i$
$\underline{k}$	unit vector, z direction
$n$	refractive index of light
$\underline{n}$	outward normal to surface
$\underline{n}'$	inward normal to surface
$p$	path length
$r$	radion
$\underline{r}$	position vector
$r_i$	reflectance of $i$ th surface
$R_{ab}$	cross correlation function of $a$ and $b$
$\text{Re}$	real part of expression within braces
$s$	integer, switch number
$s(t)$	signal
$\hat{s}(t)$	Hilbert transform of $s(t)$
$t, t_0, t$	time
$t_i, t_r$	transmittance
$t_p$	pulse duration
$T$	transit time of cell
$U(x,t)$	light intensity distribution
$U_1(x,t)U_2(x,t)$	correlator output light intensity

$v$	velocity of sound in cell
$V$	signal intensity
$W$	plane width
$x$	spatial coordinate parallel to sound propagation in Bragg cell
$z$	spatial coordinate perpendicular to sound propagation in Bragg cell
$z(t)$	analytic signal corresponding to $s(t)$
$Z(\omega)$	the Fourier transform of $z(t)$
$\alpha_{ij}$	angle between surface $i$ and surface $j$
$\alpha(t)$	phase angle
$\alpha, \beta, \gamma$	general angles
$\Delta$	variation of parameter following
$\epsilon(t)$	the envelope of $z(t)$
$\theta_1, \theta_2, \theta_3$	general angles
$\theta_i$	incidence angle
$\theta_B$	Bragg angle
$\Omega$	wavelength of sound
$\lambda$	wavelength of light in medium
$\lambda_0$	wavelength of light in vacuo
$\tau$	time
$\nu$	frequency of light
$\phi$	beam divergence
$\psi$	general angle
$\omega$	angular frequency = $2\pi f$

REFERENCES

No.	Author	Title
1	Sprague, R.A.	"A Review of Acousto-Optic Signal Correlators". Optical Engineering Vol 16, September/October 1977
2	Sprague, R.A. and Koliopoulos, G.L.	"Time Integrating Acousto-optic Correlator". Applied Optics Vol 15, No. 1, January 1976
3	Rhodes, W.T.	"Acousto-Optic Signal Processing: Convolution and Correlation". Proc. IEEE, Vol 69, No. 1, January 1981
4	Kellman, P.	"Time Integrating Optical Signal Processing". SPIE Vol 214 Acousto Optic Bulk Wave Devices, 1979
5	Guilfoyle, P.S.	"1979 Time Integrating Optical Processors in One Dimension". SPIE, Vol 214 Acousto-optic Bulk Wave Devices, 1979
6	Gottlieb, M., Conroy, J.J. and Foster, T.	"Opto-acoustic Processing of Large Time-Bandwidth Signals". Applied Optics Vol 11, No. 5, May 1972
7	Casseday, M.W., Berg, N.J., Abramowitz, I.J. and Lee, J.N.	"Wide Band Signal Processing Using the Two-Beam Surface Acoustic Wave Acousto-optic Time Integrating Correlator". IEEE Transactions on Sonics and Ultrasonics, Vol SU-28, No. 3, May 1981
8	Papoulis, A.	"Systems and Transforms with Applications in Optics". New York, McGraw Hill, 1968
9	Goodman, J.W.	"Introduction to Fourier Optics". New York, McGraw Hill, 1968
10	Klein, W.R. and Cook, B.D.	"Unified Approach to Ultrasonic Light Diffraction". IEEE Transactions on Sonics and Ultrasonics, July 1967
11	Fogg, D.A.B., and Varney, R.W.	"A Bragg cell Mathematical Model". DRCS programme package, EWS Group ERL, 1983
12	Venning, J.R.	"The Spectral Characteristics of Metal Beam Splitters". DSTO ERL Technical Report ERL-0123-TR

No.	Author	Title
13	Fogg, D.A.B.	"The Use of Phase shift Keying in Bulk Acousto Optic Devices". DRCS Technical Report to be published
14	Cook, C.E. and Bernfeld, M.	"Radar Signals, an Introduction to Theory and Application". Academic Press, New York, 1967
15	Turin, G.L.	"An Introduction to Matched Filters". IRE Transactions on Information Theory, June 1960
16	Casasent, D. and Silbershatz, G.	"Product Code Processing on a Triple-product Processor". Applied optics Vol 21, No. 11, June 1982
17	Vijaya Kumar, B.V.K. and Casasent, D.	"Space-Blur Bandwidth Product in Correlator Performance Evolution". J.Opt.Soc. Am Vol 70, No. 1, January 1980
18	Goutzoulis, A.P. and Vijaya Kumar, B.V.K.	"Optimum Time Integrating Acousto Optic Correlator for Binary Codes". Optics Communications, Vol 48, No. 6, January 1984
19	Crepeau, P.J.	"Fundamentals of Covert Communications". NRL Memorandum Report 2873, July 1974
20	Hecht, D.L.	"Multifrequency Acousto-optic Diffraction". IEEE Transactions on Sonics and Ultrasonics Vol SU-24, No. 1, January 1977
21	Hecht, D.L.	"Spectrum Analysis using Acousto optic Devices". Optical Engineering Vol 16, No. 5, September/October 1977
22	Preston, K. Jnr	"Coherent Optical Computers". McGraw Hill
23	Kellman, P., Shaver, H.N. and Murray, J.W.	"Integrating Acousto Optic Channelised Receivers". Proceedings of the IEEE, Vol 69, No. 1, January 1981

APPENDIX I

DETERMINATION OF PRISM CHARACTERISTICS

I.1 Prism angles

The prism has two horizontal faces and five vertical faces (see figure 4). Specification of any four angles between faces determines the prism. The two input beams are shown figure 11. The requirement that the two outgoing beams (one reflected, and one reflected and refracted) should be divergent at four times the Bragg angle  $\theta_B$ , is used to determine the prism shape.

Two rays are considered. ABCDE (see figure 11) enters surface 3 normally at the point B. This intercepts surface 2 at C making an angle  $\gamma$  with the internal normal  $\underline{n}_2$ . It is reflected towards surface 1 intercepting it at D and is refracted out of the prism to E where it is required to make an angle of  $2\theta$  with the reference line through D parallel to the top edge of surface 3. The angle the emerging ray makes with the normal to surface 1 is denoted by  $\beta$ . The second ray considered is FGH which intercepts surface 1 and G and is reflected to H making an angle  $\alpha$  with the normal to surface 1 and is required to make an angle  $2\theta$  with the reference line through G parallel to the top edge of surface 3.

The two rays considered are initially parallel so that the angle FGH is  $2\alpha$ ,  $\widehat{FGH} = \pi/2$ ,  $\widehat{IGH} = 2\theta_B$  and  $\widehat{FGH} = \widehat{FGI} + \widehat{IGH}$  so that

$$\alpha = \pi/4 + \theta_B \quad (I.1)$$

The angle  $\widehat{FGJ} = \pi/2 - \alpha$  and  $\widehat{FGJ} + \widehat{DGI} = \pi/2$  so that  $\widehat{DGI} = \widehat{PDK} = \alpha$ . Also  $\widehat{PDK} + \widehat{KDE} + \widehat{EDn}_1 = \pi/2$ , which implies that

$$\beta = \pi/2 - \alpha - 2\theta_B$$

Using equation (I.1) this becomes

$$\beta = \pi/4 - 3\theta_B \quad (I.2)$$

The angle  $\widehat{CDn}_1$  is denoted by  $\beta'$ . Noting that  $\widehat{JIG} = \pi/2 - \alpha$  and summing the angles of the triangle QCD an expression involving  $\gamma$  can be written, namely  $2\gamma = \pi - (\pi/2 - \beta') - (\pi/2 - \alpha)$  so that

$$\gamma = \frac{1}{2} (\beta' + \alpha) \quad (I.3)$$

Denoting  $\widehat{MCN}$  by  $\zeta$  and  $\widehat{CDL}$  by  $\psi$  it is clear that  $\widehat{CDL} = \widehat{DCN}$  and  $\zeta + \psi + \gamma = \pi/2$ . Noting that  $\widehat{LDn}_1 = \widehat{n}_1DK$  implies  $\psi = \pi/2 - \beta' - \alpha$ . The angle  $\alpha_{12}$  between surfaces 1 and 2 can now be found.  $\alpha_{12} = \widehat{MCN}$  or  $\alpha - \zeta$  so that

$$\alpha_{12} = \alpha - (\pi/2 - \psi - \gamma) \quad (I.4)$$

Substituting for  $\psi$  and  $\gamma$  and noting that  $\sin\beta/\sin\beta' = n$ , the refractive index of the glass, the expression for  $\alpha_{12}$  becomes

$$\alpha_{12} = \alpha/2 - \frac{1}{2} \sin^{-1} (1/n \sin\beta) \quad (\text{I.5})$$

Substituting for  $\alpha$  and  $\beta$ ,

$$\alpha_{12} = \pi/8 + \frac{1}{2} \theta_B - \frac{1}{2} \sin^{-1} [1/n \sin (\pi/4 - 3\theta_B)] \quad (\text{I.6})$$

The angle  $\alpha_{14}$  is determined by the fact that the ray DO, the component of CD internally reflected should be normal to surface 4 to minimise strong light in the prism. Since  $\underline{n}'\hat{D}O = \beta'$  it follows that  $\alpha_{14} = \beta'$  or  $\alpha_{14} = \sin^{-1} (1/n \sin\beta)$  so that substituting for  $\beta$

$$\alpha_{14} = \sin^{-1} [1/n \sin (\pi/4 - 3\theta_B)] \quad (\text{I.7})$$

The internal prism angle  $\alpha_{13}$  between surfaces 1 and 3 is simply  $\alpha_{13} = \pi - \alpha$  or

$$\alpha_{13} = 3\pi/4 - \theta_B \quad (\text{I.8})$$

Surface 5 is arbitrary and is defined to be normal to surface 3, ie  $\alpha_{35} = \pi/2$ . The length of surface 2 is such that the refracted ray at G intercepts surface 4 not surface 2. The angle  $\alpha_{32}$  is equal to  $\gamma$  so that from 3, and substituting for  $\alpha$ ,  $\beta'$  and  $\beta$

$$\alpha_{32} = \frac{1}{2} \sin^{-1} [1/n \sin (\pi/4 - 3\theta_B)] + (\pi/8 + \frac{1}{2} \theta_B) \quad (\text{I.9})$$

$$\alpha_{42} = \pi - \alpha_{21} - \alpha_{41}$$

As a simple check the following relationship should be true (see figure 4)

$$\alpha_{32} + \alpha_{31} + \alpha_{14} + \alpha_{42} = 360^\circ$$

Using the refractive index of  $n = 1.51509$  of the BK7 glass out of which the prism was made, the angles are calculated to be:

$$\begin{aligned} \alpha_{32} &= 36^\circ 17' 28'' \\ \alpha_{31} &= 134^\circ 35' 56'' \\ \alpha_{14} &= 27^\circ 10' 52'' \\ \alpha_{42} &= 161^\circ 55' 44'' \end{aligned}$$

and the sum is found to be  $360^{\circ} 0' 0''$  as required.

### I.2 Phase equalisation

There is a phase difference between the two collinear first order beams  $+1_A$ ,  $+1_B$  (see figures 1(a) and 2) reaching the TIC correlator detector. This is due to their different optical path lengths both in the prism and in the cells. Moving the prism parallel to surface 2 effectively alters the prism thickness. (Length of normal from surface 2 to surface 1 at the point under consideration) and proportionally changes the path length of one beam. However, the movement required for  $2\pi$  change in phase is only  $\lambda/32$  (approximately) or 20 nm. This is therefore not a practical way of equalising phase.

A phase plate of dimension  $1 \times 1 \text{ cm} \times 0.2 \text{ mm}$ , coated for improved transmission at  $\lambda = 632.8 \text{ nm}$  was used. This was placed in the beam directed towards surface 1. If the width of the plate is  $W$  and the rotation angle is  $\theta$  the optical path change  $\Delta p$  is given by

$$\Delta p = n'W(1 - \cos \theta)/\cos \theta$$

where  $n$  is the refractive index of the plate. For example a 2 mm thick plate requires a rotation  $1^{\circ} 10' 36''$  to change the phase of  $\lambda = 632.8 \text{ nm}$  light by  $2\pi$ .

### I.3 Prism rotation functions

Rotation of the prism relative to the incident light (ie increasing the angle of incidence) changes the directions of both outgoing beams. They do not vary by the same amount resulting in a change in the divergence of the two beams.

Consider a rotation of the prism through a small angle  $\Delta\theta$  in an anticlockwise direction. The new angle of incidence  $\alpha_n$  on surface 1 for the reflected ray (see figure 12(a)) is given simply by  $\alpha_n = \alpha + \Delta\theta$  and the angle  $\phi_1$  which the outgoing reflected ray makes with the reference (top edge of surface 3) is given by  $2\alpha_n - \pi/2$  or substituting for  $\alpha_n$  and then  $\alpha$ .

$$\phi_1 = 2\theta_B + 2\Delta\theta \quad (\text{I.10})$$

The ray entering surface 3 is now not normal and suffers a refraction. From figure 13(b) the following relations can readily be obtained.

$$\zeta_1 = \pi/2 - \alpha_{32} - \Delta\theta'$$

$$\gamma_n = \pi/2 - \zeta_1 = \alpha_{32} + \Delta\theta'$$

$$\alpha_{32} + \zeta_2 + \gamma_n = \pi/2$$

Substituting for  $\gamma_n$ ,  $\zeta_2$  can be written as

$$\zeta_2 = \pi/2 - 2\alpha_{32} - \Delta\theta'$$

Also

$$\beta'_2 = \zeta_2 + \alpha + \pi/2$$

so that

$$\beta'_2 = 2\alpha_{32} + \Delta\theta' - \pi/4 - \theta_B$$

The outgoing ray makes an angle  $\phi_2$  with the reference line. Since  $\phi_2 + \beta_2 + \alpha = \pi/2$

$$\phi_2 = \pi/4 - \theta_B - \sin^{-1} \{n \sin[2\alpha_{32} + \Delta\theta' - \pi/4 - \theta_B]\}$$

Substituting for  $\alpha_{32}$  from equation (I.9)

$$2\alpha_{32} - \pi/4 - \theta_B = \sin^{-1} [1/n \sin(\pi/4 - 3\theta_B)]$$

so that  $\phi_2$  is given by

$$\phi_2 = \pi/4 - \theta_B - \sin^{-1} \{n \sin(\sin^{-1} [1/n \sin(\pi/4 - 3\theta_B)] + \Delta\theta')\} \quad (I.11)$$

where

$$\Delta\theta' = \sin^{-1} [1/n \sin \Delta\theta]$$

Note that when  $\Delta\theta = 0$ ,  $\Delta\theta'$  will also be zero and the equations (I.10) and (I.11) reduce simply to

$$\phi_1 = \phi_2 = 2\theta_B$$

as required.

The divergence  $\phi$  between the two outgoing rays is just the sum  $\phi_1 + \phi_2$ . For small  $\Delta\theta$ ,  $\phi$  is given approximately by a simple linear relationship

$$\phi = C_0 \Delta\theta + C_1$$

For the manufactured prism  $C_0 = 0.78 (\pm 0.02)r$  and  $C_1 = 0.028 r (=4\theta_B)$ .

APPENDIX II

REVIEW OF PERFORMANCE PARAMETERS

II.1 Processing gain

Since the AO, TIC is essentially a matched filter the well known assessments of matched filter performances(ref.14,15) are applicable. The system performance criterion is processing gain, PG, defined to be the ratio of the output signal to noise ratio, SNR<sub>o</sub> to the input signal to noise ratio SNR<sub>i</sub>. By definition(ref.14).

$$SNR_o = \frac{\text{peak instantaneous output signal power}}{\text{output noise power}}$$

which for a matched filter can be shown to be(ref.14),  $2E/kN_o$ , where E is the received signal energy and  $N_o/2$  is the noise spectral density (in watts/cycle/second). The constant k is near unity and will be considered equal to 1 here. Consider the noise to be white and define the noise bandwidth B of the matched filter as the bandwidth of a rectangular filter with the same maximum gain and the same output noise power as the matched filter. Then

$$SNR_i = \frac{\text{average signal power at the filter input}}{\text{noise power in the matched filter band}} = \frac{E/T}{BN_o}$$

where T is the effective duration of the signal. The processing gain is given by  $PG = SNR_o/SNR_i = 2 TB$ .

A number of specific treatments of PG in TICs exist(ref.16 to 19, and 23). It is relevant to review that of reference 17. This deals with the case of additive stationary, zero mean Gaussian noise. The output signal to noise ratio is defined in terms of the mean and variance of the autocorrelation function.

$$R(\tau) = \frac{1}{T_I} \int_{T_I} [s(t - x/V) + n(t)] s(t) dt$$

The mean is the maximum value  $P_s$  of the autocorrelation function and the variance is found to be

$$\text{var} = E \left[ \left\{ \int_{T_I} n(t + \tau) s(t) dt \right\}^2 \right]$$

so that

$$PG = \frac{\text{mean/var}}{SNR_i}$$

When the ratio of the bandwidth of the noise to the bandwidth of the signal is small (ie for a narrow band jammer) the conventional PG is obtained. Reference 18 quotes the above definition of PG and derives expressions in terms of  $SNR_i$  and time bandwidth product for a number of correlators. These types of expression are useful for comparison purposes.

## II.2 Dynamic range

In practice only a fraction of the large time bandwidth capability of a TIC can be used. The system is limited by the dynamic range of the output detector array(ref.1).

The Bragg cell has an inherent dynamic range. This is determined by the difference between signal intensity and noise sources. The most significant noise sources are the third order intermodulation components  $2f_i - f_j$  formed from frequencies  $f_i$  and  $f_j$  which may be present in the cell. In the Bragg regime this intermodulation intensity is given(ref.20) by  $|J_3(V)|^2 \approx (V/2)^6$  where the intensity of both signals are equal to  $V$ , and  $J_3$  is a third order Bessel function. A graph showing the limits on Bragg cells inherent dynamic range for this case is shown in figure 7. Some of the analytic results were verified using a Bragg cell mathematical model(ref.10,11).

The lower limit is due to optical noise due mainly to diffraction at the aperture restricting the beam. Other optical noise sources are discussed in reference 22. If  $N$  is the number of resolvable frequencies (bandwidth divided by resolution,  $= B\tau$ ) then the optical background is(ref.21).

$$I_{\min}/I_o = (1/\pi N)^2$$

For this prototype,  $B = 30$  MHz,  $\tau = 3$   $\mu$ s, so that  $B\tau = 90$  and the optical background  $\approx 10^{-5}$ . For a more representative  $N$  of say 1000 this would be  $\approx 10^{-7}$ . The limiting dynamic range is that of the detector array. This point was discussed in Section 6 of the main text.

## II.3 Resolution

The divergence  $\alpha$  of the first order from the incident beam is given by

$$\alpha = \frac{\lambda}{\Lambda} = \frac{\lambda f_s}{v}$$

where  $f_s$  and  $v$  are the frequency and speed respectively of the sound in the cell. Varying the frequency will vary  $\alpha$  so that,  $\Delta x = \lambda \Delta f_s / v$ .

If a light beam passes through an aperture  $D$  there is an unavoidable diffraction spread  $\alpha_{\min} = \lambda/D$ . Since

$$\frac{\text{maximum angular diffraction}}{\text{angular resolution}} = \frac{\text{frequency range}}{\text{frequency resolution}}$$

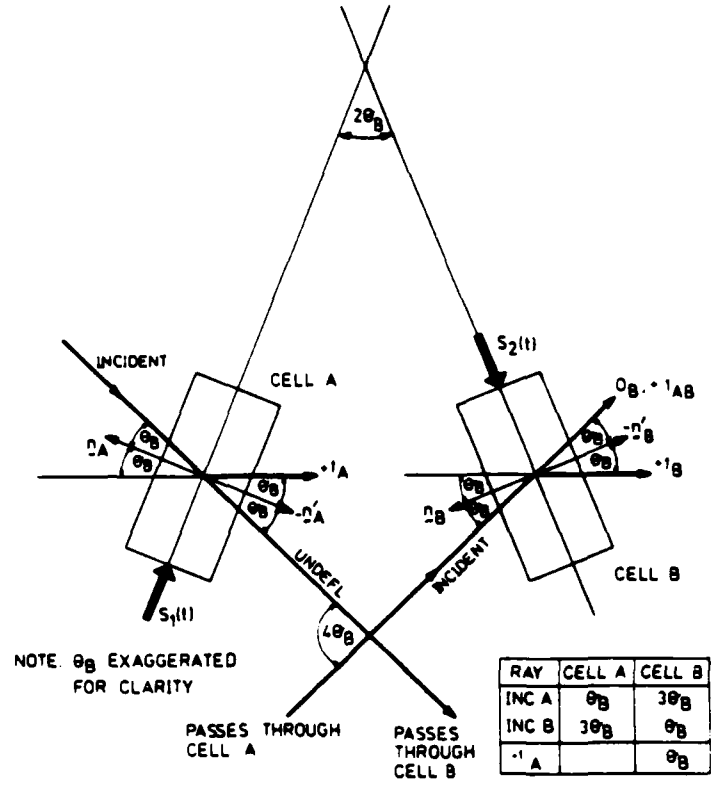
or

$$\frac{\Delta\alpha}{\alpha_{\min}} = \frac{\Delta f}{\delta f}$$

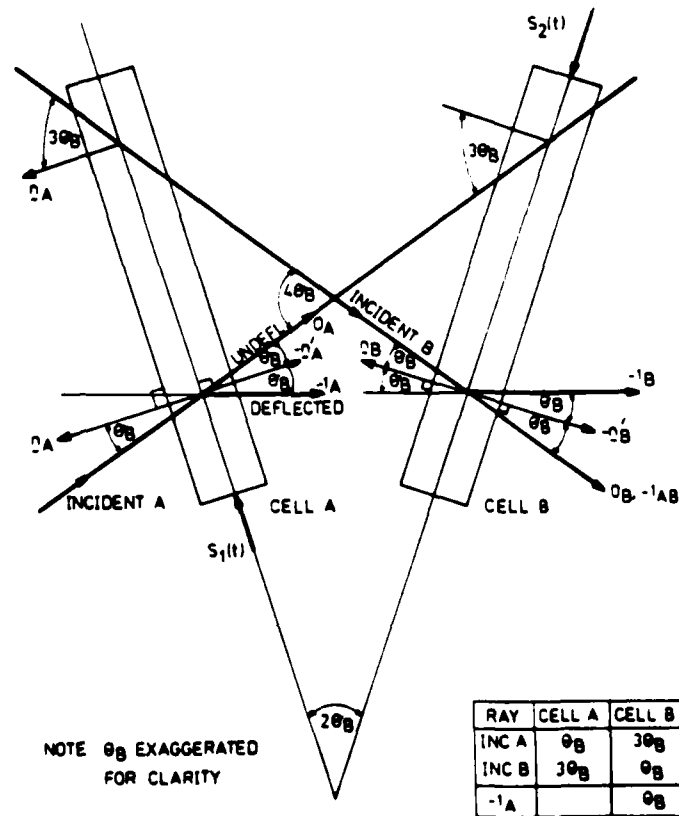
then

$$\delta f = v/D .$$

In a modulator the beamwidth  $D$  is small. In a deflector it is usually the maximum cell aperture. In the latter case the transit time  $\tau = D/v$  so that  $\delta f = 1/\tau$ .



(a) Upshifted first orders



(b) Downshifted first orders

Figure 1. Bragg cell orientation

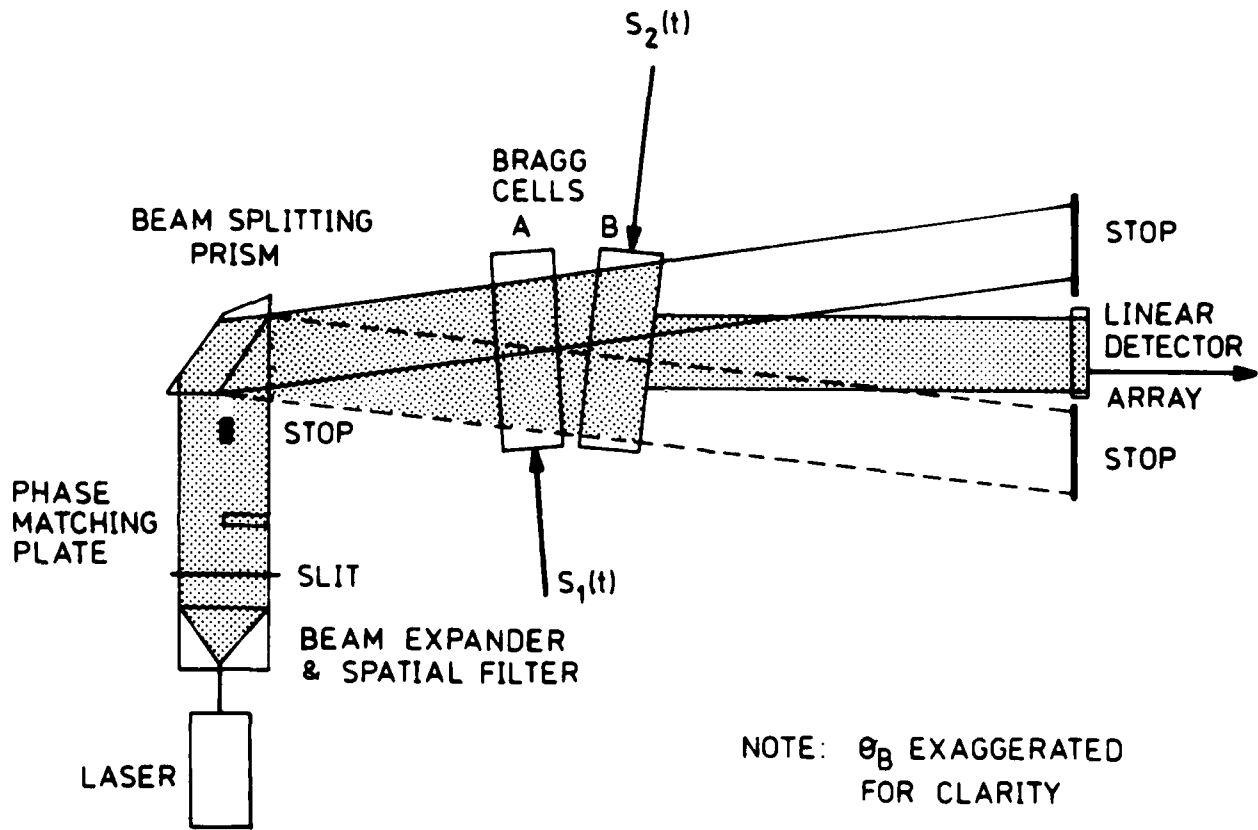


Figure 2. Bulk AO TIC correlator architecture

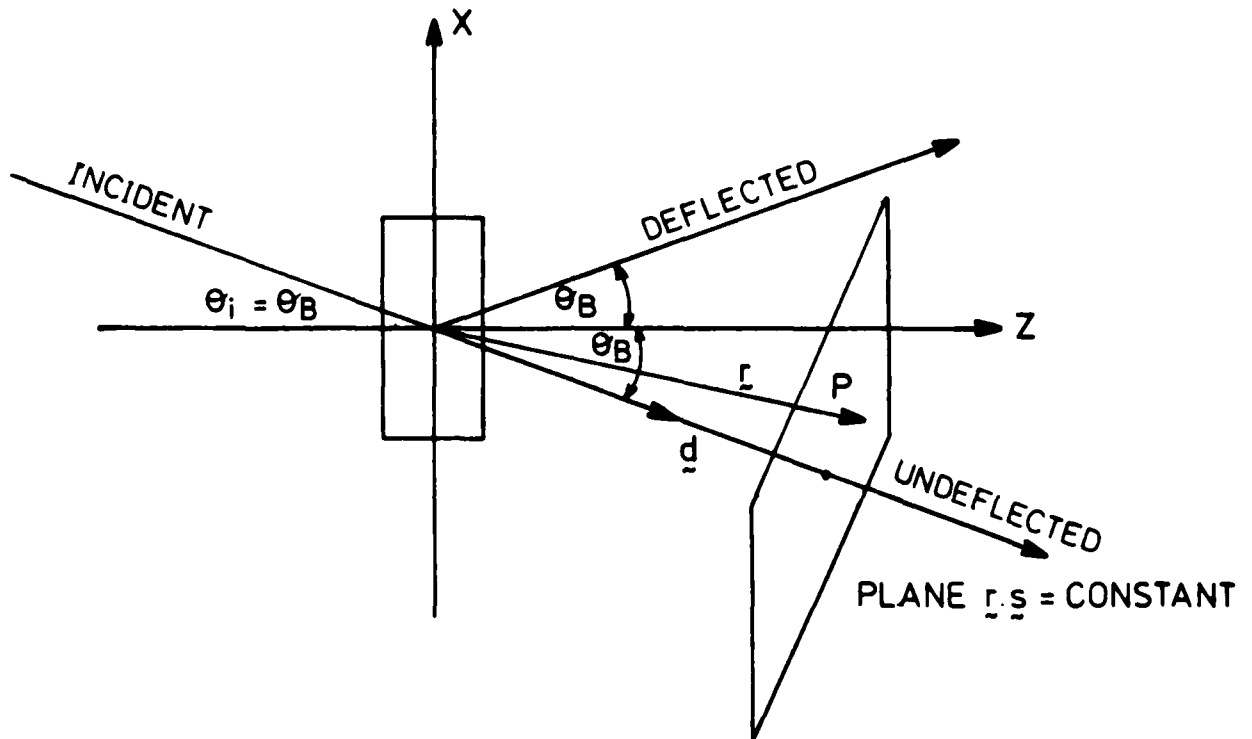


Figure 3. Bragg cell optics

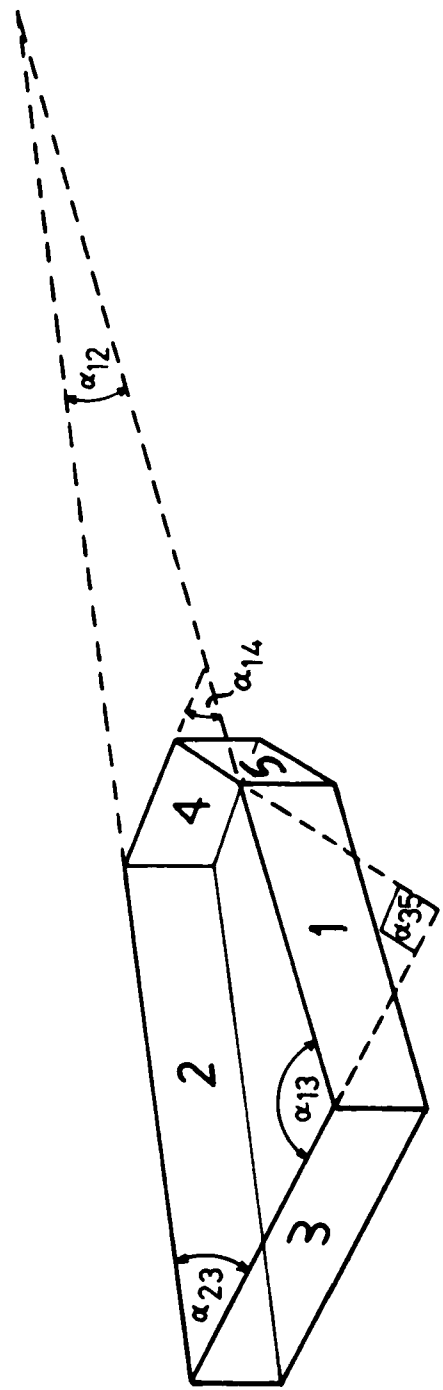


Figure 4. The prism

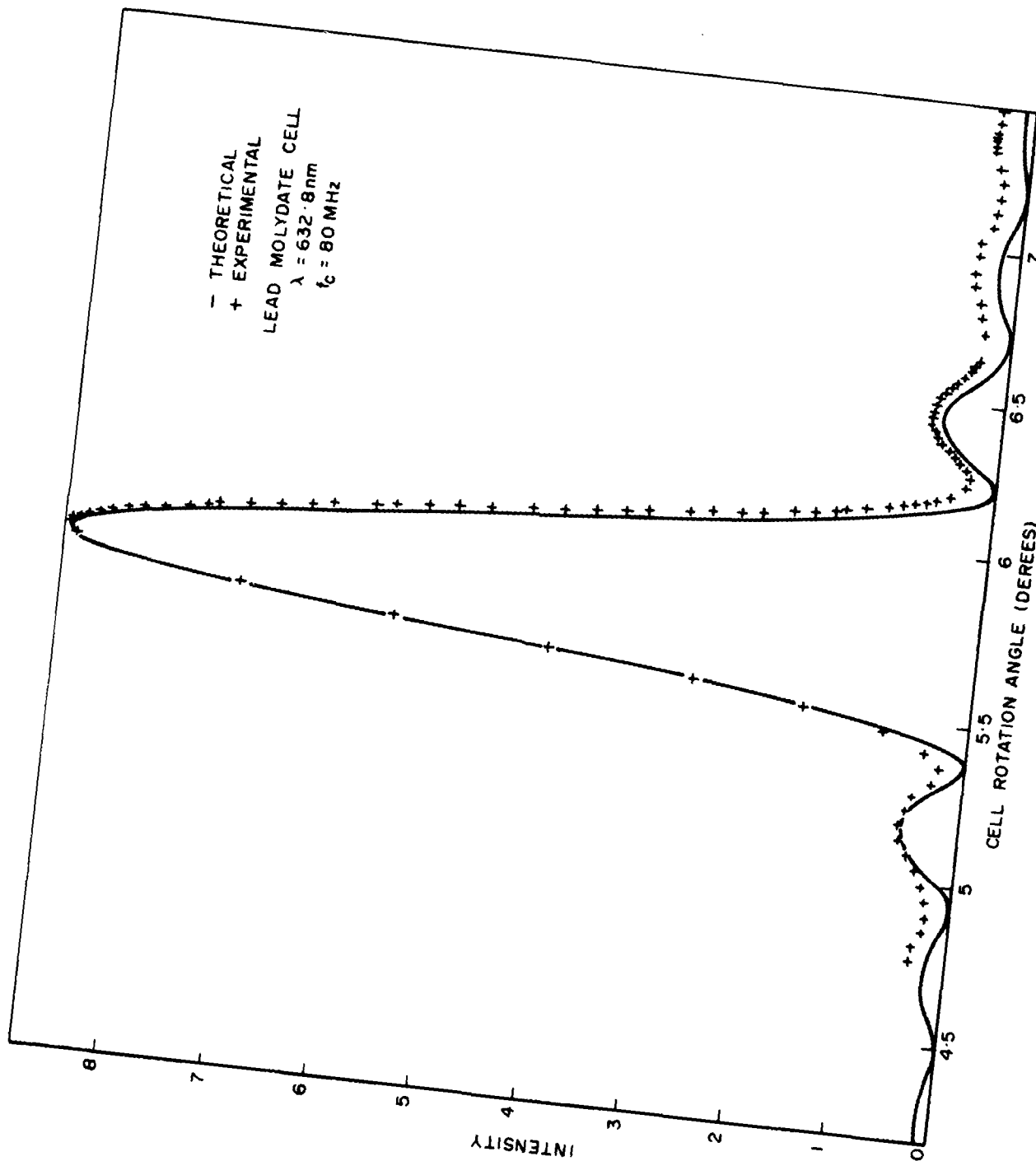
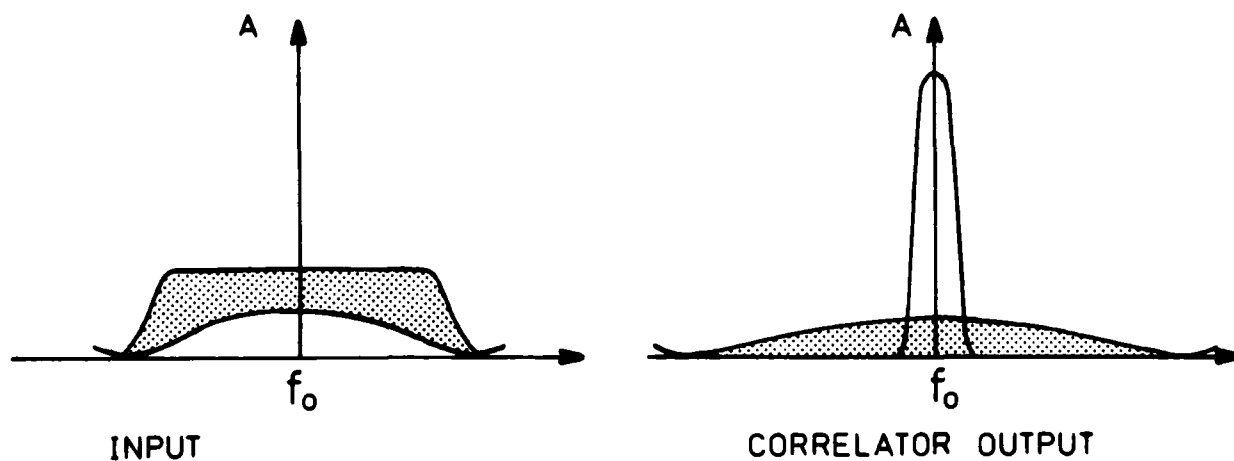
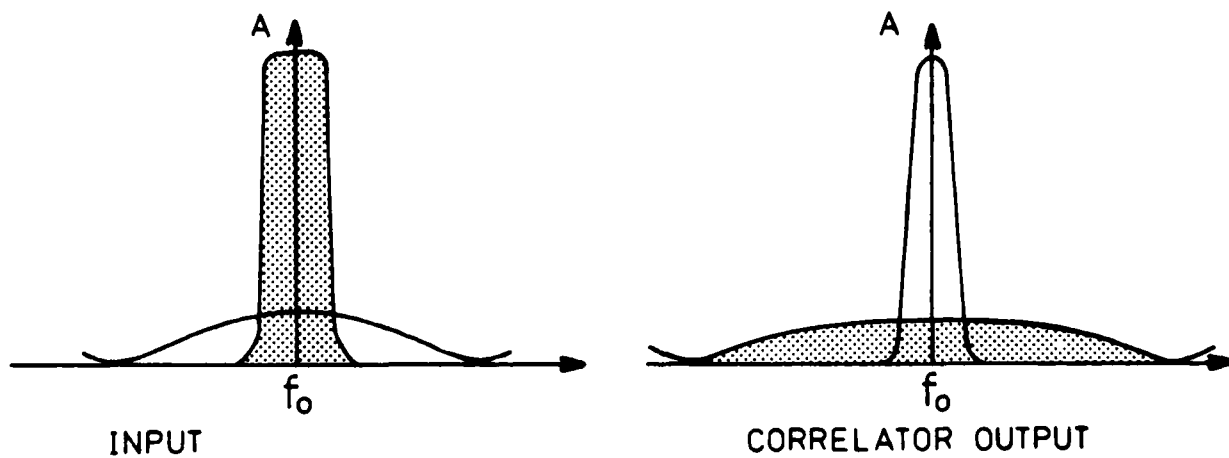


Figure 5. Incidence angle sensitivity



(a) SS SIGNAL, WIDEBAND NOISE



(b) SS SIGNAL, NARROWBAND NOISE

KEY:  SIGNAL  
 NOISE

Figure 6. Signal and noise spectra

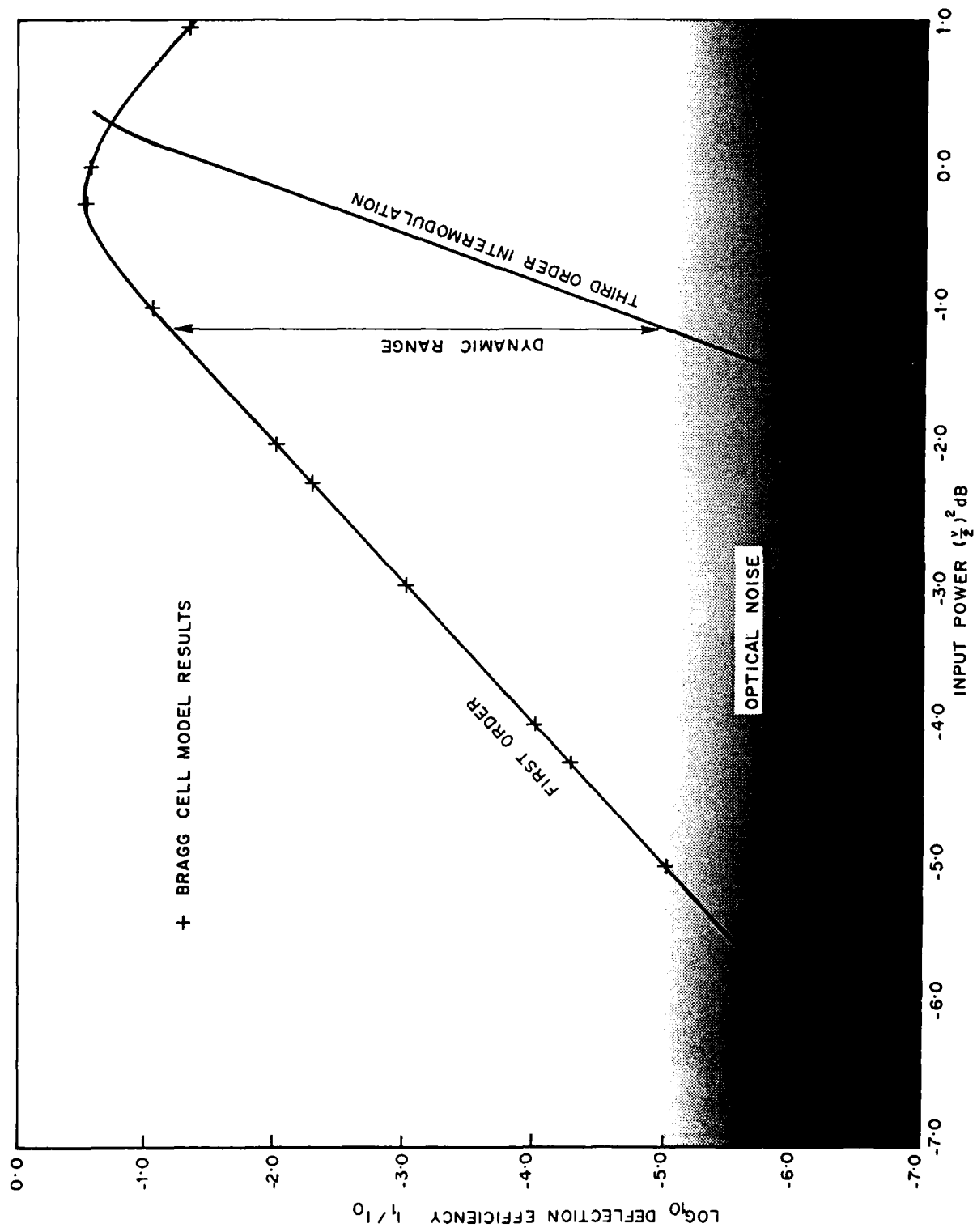
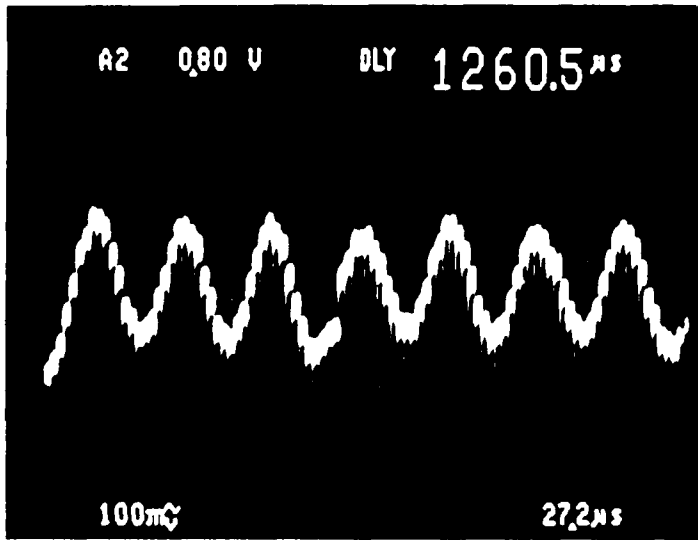


Figure 7. Dynamic range limits, two tone case



CARRIER FREQUENCY 80MHz  
CHIP RATE 20MHz  
100mv / DIV

Figure 8. Correlator output for an OOK signal

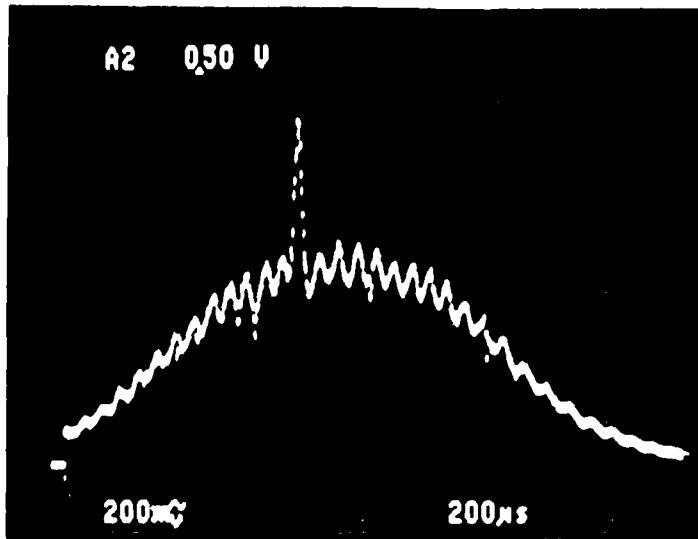


Figure 9(a). Correlator output for a spread spectrum signal

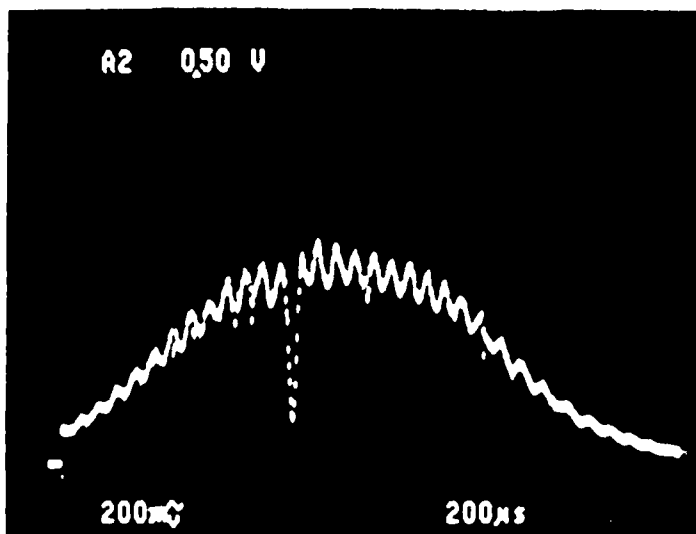


Figure 9(b). Phase shifted output for pedestal subtraction

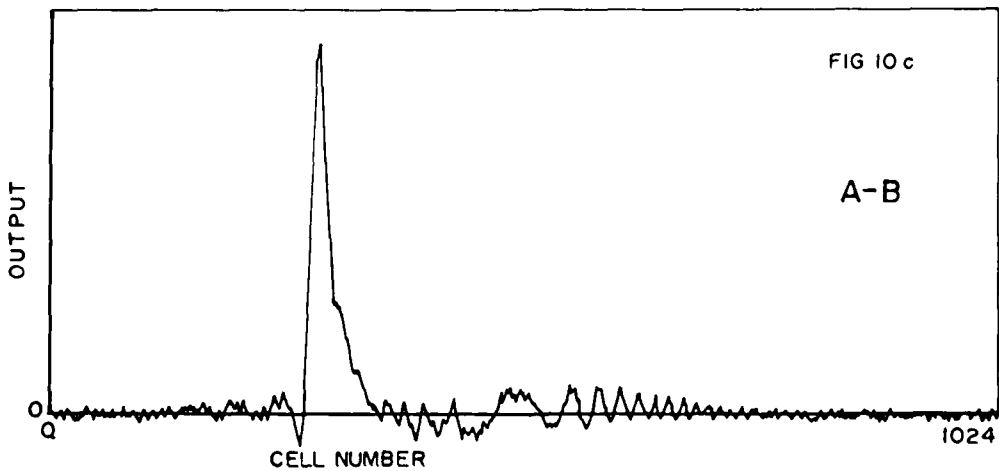
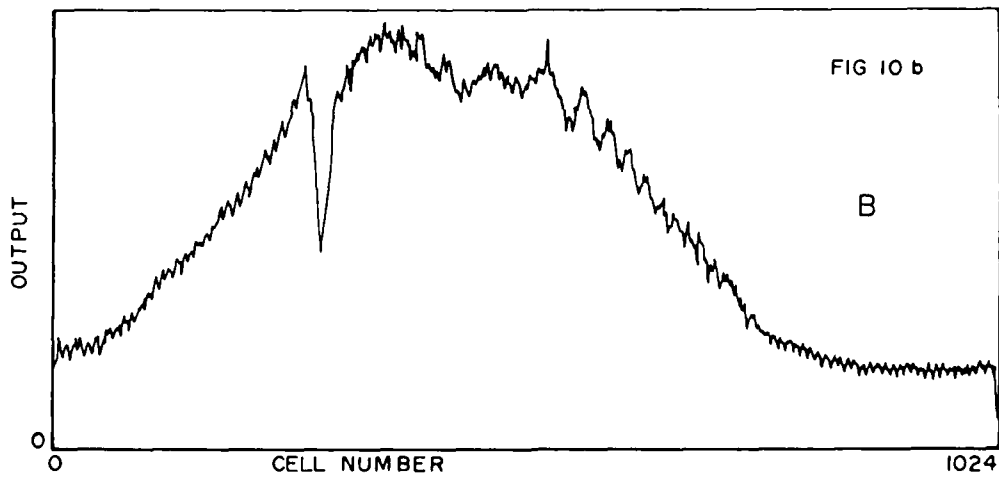
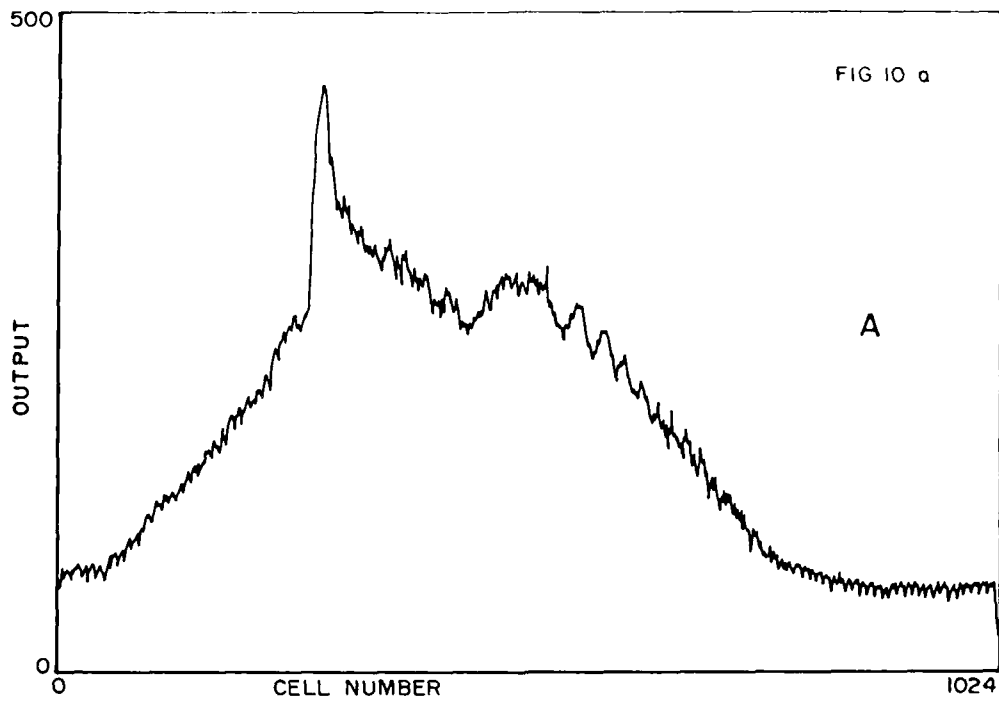


Figure 10. Correlation peak after digital subtraction

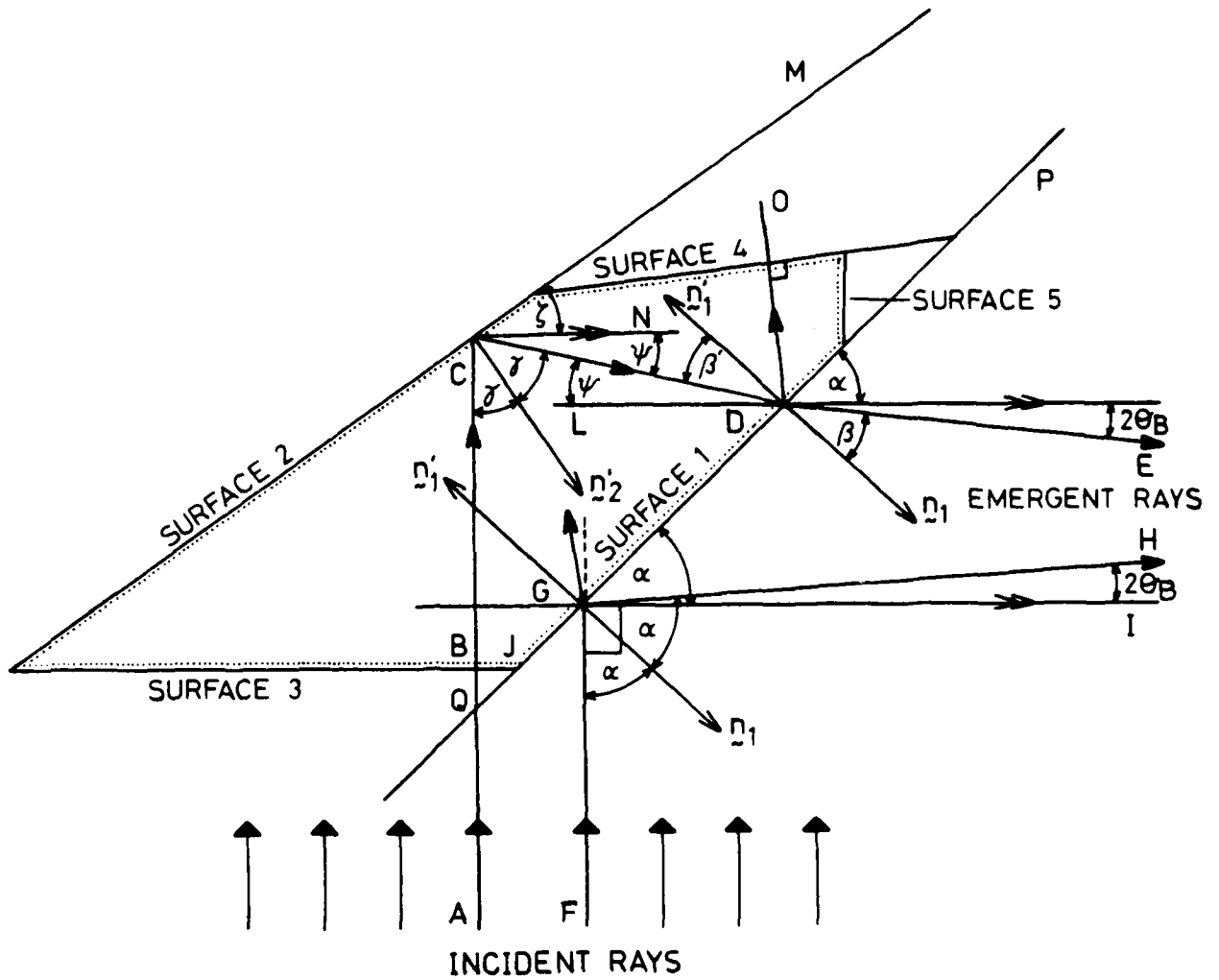
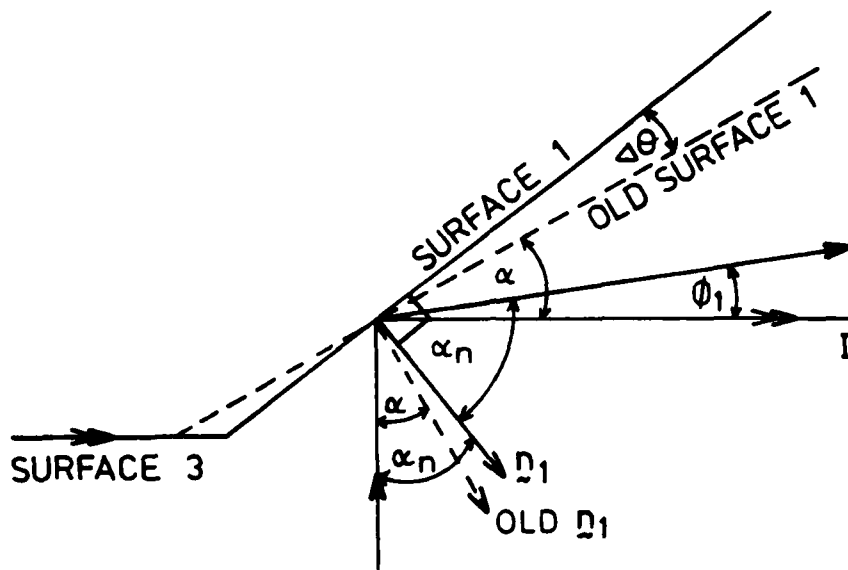
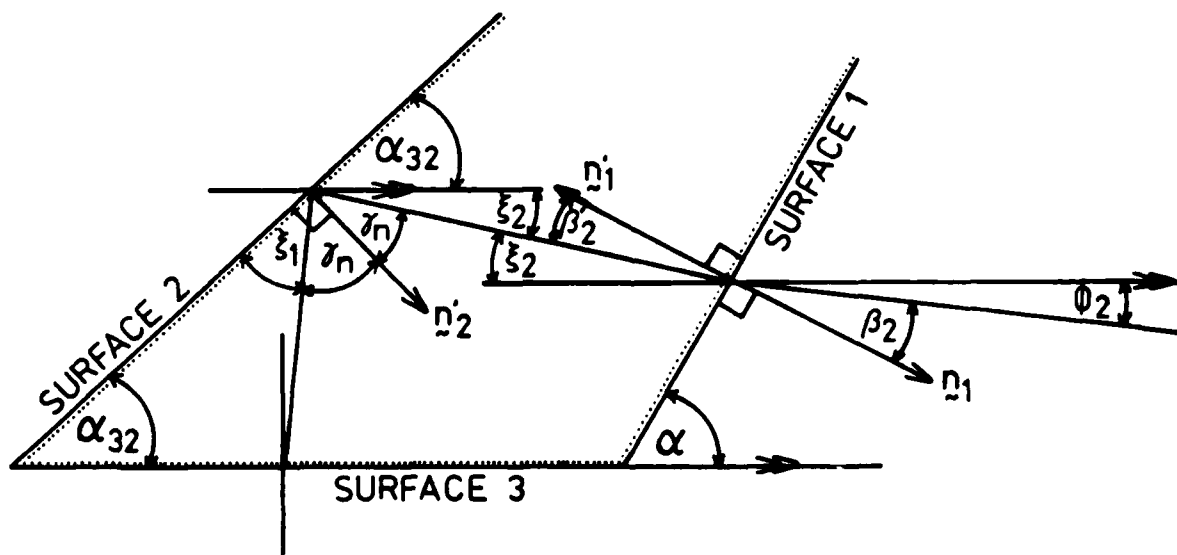


Figure 11. Prism geometry



(a) The reflected ray



(b) The refracted ray

Figure 12. Prism rotation geometry

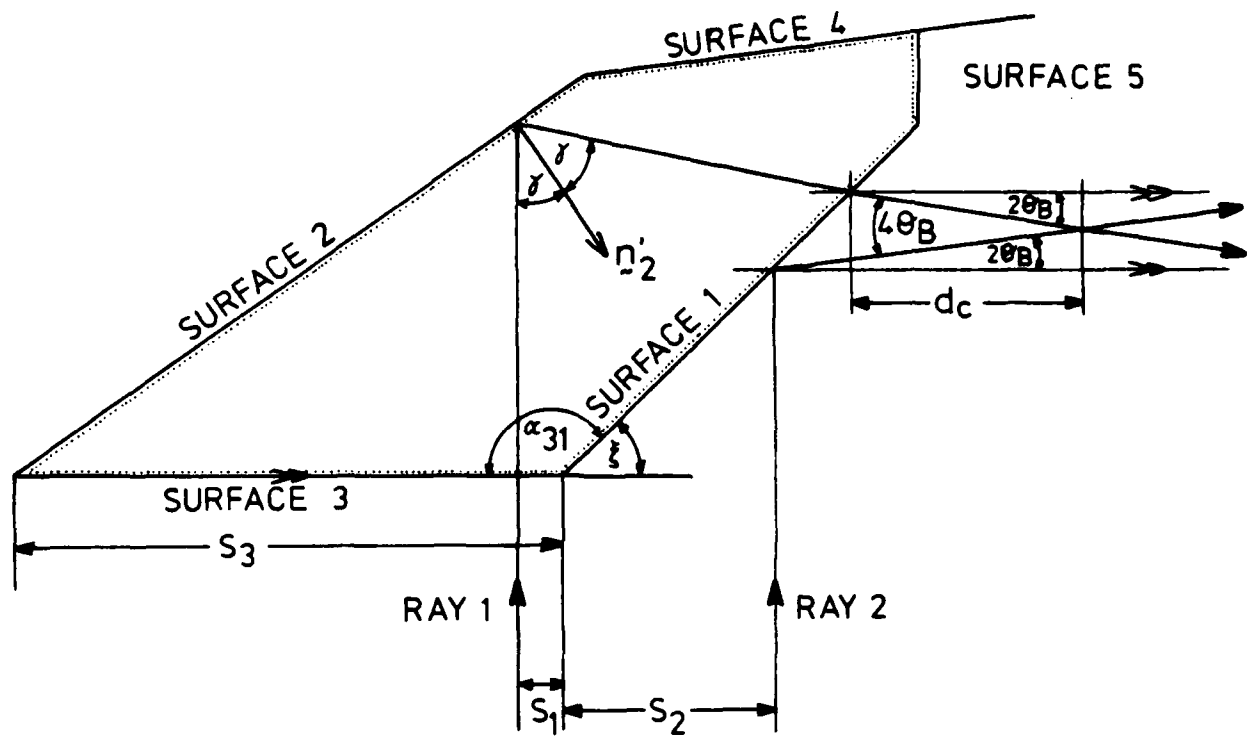


Figure 13. Crossover distance

DISTRIBUTION

Copy No.

EXTERNAL

In United Kingdom

Defence Science Representative, London	Cnt Sht Only
Institute of Electrical Engineers	1
Brisish Library, Lending Division, Boston Spa, Yorks	2

In the United States of America

Counsellor, Defence Science, Washington	Cnt Sht Only
Engineering Societies Library	3

In Australia

Department of Defence

Chief Defence Scientist	}	4
Deputy Chief Defence Scientist		
Controller, External Relations, Projects and Analytical Studies		
Superintendent, Science Programs and Administration		

Director, Joint Intelligence Organisation	5
---	---

Document Exchange Centre  
 Defence Information Services Branch for:

Microfilming	6
--------------	---

United Kingdom, Defence Research Information Centre (DRIC)	7 - 8
--	-------

United States, Defense Technical Information Center	9 - 20
---	--------

Canada, Director, Scientific Information Services	21
---	----

New Zealand, Ministry of Defence	22
----------------------------------	----

National Library of Australia	23
-------------------------------	----

Defence Library, Campbell Park	24
--------------------------------	----

Library, Materials Research Laboratories	25
--	----

Library, H Block, Victoria Barracks, Melbourne	26
--	----

Library, RAN Research Laboratory	27
----------------------------------	----

Library, Aircraft Research and Development Unit	28
---	----

Library, Aeronautical Research Laboratories	29
Director General, Army Development (NSO), Russell Offices for ABCA Standardisation Officers	
UK ABCA representative, Canberra	30
US ABCA representative, Canberra	31
Canada ABCA representative, Canberra	32
NZ ABCA representative, Canberra	33
Deputy Secretary (Manufacturing)	}
Deputy Secretary (Materiel and Resources)	
Controller, Defence Aerospace Division	
Controller, Munitions Division	
Library, DDS Central Office	35
Director, Industry Development, SA/NT	Cnt Sht Only

WITHIN DRCS

Director, Electronics Research Laboratory	36
Superintendent, Optoelectronic Division	37
Superintendent, Electronic Warfare Division	38
Senior Principal Research Scientist, Electronic Warfare Division	39
Principal Officer, Information and Signal Processing Group	40
Principal Officer, Electronic Warfare Techniques Group	41
Principal Officer, Communications Electronic Warfare Group	42
Principal Officer, Infrared and Optical Countermeasures Group	43
Principal Officer, Optical Techniques Group	44
Principal Officer, Communications Technology Group	45
Principal Officer, Optoelectronic Device Physics Group	46
Principal Officer, Signal Processing and Classification Group	47
Dr R.M. Hawkes, Information and Signal Processing Group	48
Dr I.G. Fuss, Information and Signal Processing Group	49
Dr S.T. Hood, Information and Signal Processing Group	50
Mr A.D. Doolette, Information and Signal Processing Group	51

Mr J.R. Venning, Optical Techniques Group

52

Author

53

DRCS Library

54 - 55

Spares

56 - 61

## DOCUMENT CONTROL DATA SHEET

Security classification of this page

UNCLASSIFIED

## 1 DOCUMENT NUMBERS

AR  
Number: AR-004-121Series  
Number: ERL-0325-TROther  
Numbers:

## 2 SECURITY CLASSIFICATION

a. Complete  
Document: Unclassifiedb. Title in  
Isolation: Unclassifiedc. Summary in  
Isolation: Unclassified

## 3 TITLE

A COMPACT BULK ACOUSTO-OPTIC TIME INTEGRATING CORRELATOR

## 4 PERSONAL AUTHOR(S)

D.A.B. Fogg

## 5 DOCUMENT DATE:

November 1984

6 6.1 TOTAL NUMBER  
OF PAGES6.2 NUMBER OF  
REFERENCES: 23

## 7 7.1 CORPORATE AUTHOR(S)

Electronics Research Laboratory

7.2 DOCUMENT SERIES  
AND NUMBERElectronics Research Laboratory  
0325-TR

## 8 REFERENCE NUMBERS

a. Task: DEF 82/224

b. Sponsoring  
Agency:

## 9 COST CODE:

312453/134

## 10 IMPRINT (Publishing organisation)

Defence Research Centre Salisbury

11 COMPUTER PROGRAM(S)  
(Title(s) and language(s))

## 12 RELEASE LIMITATIONS (of the document):

Approved for Public Release

Security classification of this page

UNCLASSIFIED

13 ANNOUNCEMENT LIMITATIONS (of the information on these pages):

No limitations

14 DESCRIPTORS:

a. EJC Thesaurus Terms	Acousto optics Correlators Signal processing Optoacoustic filters Optical correlators.
b. Non-Thesaurus Terms	Time integrating correlators

15 COSATI CODES:

20060  
20010

16 SUMMARY OR ABSTRACT:  
(if this is security classified, the announcement of this report will be similarly classified)

This report describes the design and testing of a prototype correlator using lead molybdate Bragg cells. It indicates the suitability of this design for cells made of materials with longer transition times, such as tellurium dioxide. Compactness and simplicity are achieved by the use of a specially designed prism: An analysis of the AO, TIC process and performance parameters is given.

The official documents produced by the Laboratories of the Defence Research Centre Salisbury are issued in one of five categories: Reports, Technical Reports, Technical Memoranda, Manuals and Specifications. The purpose of the latter two categories is self-evident, with the other three categories being used for the following purposes:

- Reports : documents prepared for managerial purposes.
- Technical Reports : records of scientific and technical work of a permanent value intended for other scientists and technologists working in the field.
- Technical Memoranda : intended primarily for disseminating information within the DSTO. They are usually tentative in nature and reflect the personal views of the author.

**END**

**FILMED**

8-85

**DTIC**